

Broken Cloud Field Approximations in the Longwave

*E. E. Takara and R. G. Ellingson
University of Maryland
College Park, Maryland*

Abstract

Because clouds play an important role in the earth's radiation energy budget, improving the cloud models in general circulation models (GCMs) is a necessary step for climate studies. In partially cloudy skies, the geometric and optical properties of individual cloud elements need to be considered. In general, GCMs ignore the geometry of ice clouds and water clouds. They also ignore the optical properties of water clouds, modeling them as blackbodies. In this work, the accuracy of cloud approximations will be examined in the 8- μm to 12- μm window region. Calculations for water clouds and ice clouds of two geometries in two different atmospheric conditions show that the black cloud assumption is good for opaque water clouds and the GCM treatment of ice clouds can be accurate.

Introduction

Partial cloud cover is more common than completely overcast skies. Considering each cloud element in a partially overcast sky scene as a discrete entity surrounded by clear air, the partially overcast sky is field of discrete clouds separated by clear skies—a broken cloud field. To reduce this complex problem to a form suitable for climate studies, simplifying assumptions are necessary. In GCMs, $F^{\uparrow\downarrow}$, upward or downward fluxes from broken cloud fields are computed by averaging clear and overcast fluxes:

$$F^{\uparrow\downarrow} = N F^{\uparrow\downarrow}(\text{overcast}) + (1-N) F^{\uparrow\downarrow}(\text{clear}) \quad (1)$$

$F^{\uparrow\downarrow}(\text{overcast})$ and $F^{\uparrow\downarrow}(\text{clear})$ are the plane parallel solutions for completely overcast and completely clear skies. This treats broken cloud fields as sets of flat plates, accounting for the top and bottom of clouds but neglecting the cloud sides. Opaque water clouds are assumed to be black (Harshvardhan and Weinman 1982). Ice clouds are assigned an emissivity (Ebert and Curry 1992).

Computation

To compute the window region fluxes, spectral and angular integration of radiances are necessary. This is done in three steps. Once the window is divided into spectral intervals, the calculation can proceed monochromatically over each interval. The monochromatic radiance calculation consists of two parts: one outside the cloud layer, the other inside the cloud layer.

Water vapor absorption in the window is primarily due to the continuum (Kiehl 1992). Carbon dioxide and ozone are secondary absorbers. The upward and downward radiances, $I^{\uparrow\downarrow}$, were computed by summing over the wavelength (λ) intervals.

$$I^{\uparrow\downarrow} = \int_{8\mu\text{m}}^{12\mu\text{m}} I_{\lambda}^{\uparrow\downarrow} d\lambda = \sum_{i=1}^6 I_i^{\uparrow\downarrow} \Delta\lambda \quad (2)$$

$I_i^{\uparrow\downarrow}$ is the spectral radiance or specific intensity of the i^{th} wavelength interval. The intervals are: $8\mu\text{m} \leq \lambda_1 \leq 8.25\mu\text{m} \leq \lambda_2 \leq 8.75\mu\text{m} \leq \lambda_3 \leq 9.25\mu\text{m} \leq \lambda_4 \leq 10\mu\text{m} \leq \lambda_5 \leq 11\mu\text{m} \leq \lambda_6 \leq 12\mu\text{m}$.

The upward and downward flux is found by three angle Gaussian quadrature.

$$F^{\uparrow\downarrow} = \int_0^{\pi/2} I^{\uparrow\downarrow}(\theta) \cos(\theta) d\theta = \sum_{j=1}^3 w_{gj} I_i^{\uparrow\downarrow} \quad (3)$$

Upward and downward radiances outside the cloud layer are functions of gaseous transmission and emission. Within each spectral interval, the upward and downward radiances at zenith angle θ and altitudes $Z_i > Z_j$, $I^{\uparrow}(Z_i, \theta)$ and $I^{\downarrow}(Z_j, \theta)$, are given by

$$I^\uparrow(Z_i, \theta) = T(Z_i, Z_j, \theta) I^\uparrow(Z_j, \theta) + E(Z_j, Z_i, \theta) \quad (4a)$$

$$I^\downarrow(Z_j, \theta) = T(Z_i, Z_j, \theta) I^\downarrow(Z_i, \theta) + E(Z_i, Z_j, \theta) \quad (4b)$$

$T(Z_i, Z_j, \theta)$ is the transmissivity from Z_i to Z_j at zenith angle θ . $T(Z_i, Z_j, \theta) I^\uparrow(Z_j, \theta)$ is the portion of $I^\uparrow(Z_i, \theta)$ due to transmission. $E(Z_j, Z_i, \theta)$ is the portion of $I^\uparrow(Z_i, \theta)$ due to emission from Z_j through Z_i . The clear sky transmissivities, $T(Z_i, Z_j, \theta)$, and radiances, $I^\uparrow(Z_i, \theta)$ and $I^\downarrow(Z_j, \theta)$ for each model atmosphere were calculated using the Line-by-Line Radiative Transfer Model (LBLRTM; Clough et al. 1992), assuming a black surface.

The radiative transfer within the layer was modeled using the Monte Carlo method (Howell and Perlmutter 1964). In Ellingson (1982), the probability of clear line of sight (PCLoS) for a broken cloud field composed of a single layer of identical randomly overlapping cylinders at zenith angle θ was given as:

$$\begin{aligned} \text{PCLoS}(\theta) &= (1 - N) \exp(-b \tan \theta) \\ b &= -\frac{\alpha \ln(1 - N)}{\pi} \end{aligned} \quad (5)$$

N is the cloud fraction; α is the aspect ratio, cloud height over diameter (H/D). The PCLoS was used to determine if the bundle intersects the clouds.

Once it is determined whether or not the bundle intersects a cloud, the next step is to determine if the bundle is transmitted through the layer. The bundles are assigned a random number, ζ , to determine where the bundle is extinguished (absorbed or scattered). For a bundle emitted at Z_j traveling upward to Z_i

$$\text{If } \zeta \leq T(Z_i, Z_j, \theta) \text{ ; bundle is transmitted.} \quad (6a)$$

$$\text{If } \zeta > T(Z_i, Z_j, \theta) \text{ ; bundle is extinguished.} \quad (6b)$$

Bundles are tracked until they are absorbed or escape the cloud layer.

Assumptions and Parameters

Five assumptions are made. First, the cloud field is a single layer of identical randomly overlapping cylinders with a uniform cloud base altitude. Second and third, the clouds are homogenous with the same temperature profile as the surrounding air. Fourth, the temperature variation between levels is assumed to be linear. Lastly, the surface is black. The McClatchey soundings (McClatchey et al. 1971) were

used for temperature and species profiles. Results for the mid-latitude summer (MLS) and mid-latitude winter (MLW) soundings are presented here.

The fluxes are computed for two pairs of cloud aspect ratios (α) and diameter (D): the small flat cloud set, $\alpha = 0.5$; $D = 0.25$ km, cloud thickness of 0.125 km and the larger set $\alpha = 1$ and $D = 1$ km, cloud thickness of 1 km. The base cloud fraction (N), and cloud base altitude (Z_b) is also varied. N values are 0.1, 0.3, 0.5, 0.7, 0.9, and 1. Z_b values are 0.5, 2, and 4 km for water clouds, 8, 10, and 12 km for ice clouds.

The water cloud equivalent radius (R_{eq}) (Hu and Stamnes 1993) was set at 3 μm , 5 μm , and 10 μm . The liquid water content (LWC) is 0.1 g^*m^{-3} for MLW and 0.2 g^*m^{-3} for MLS. For ice clouds, the equivalent diameters (D_{eq}) ice water content (IWC) pairs were 75 μm , 0.005 g^*m^{-3} , 93 μm , 0.014 g^*m^{-3} , and 110 μm , 0.029 g^*m^{-3} . These are the Ci(1 Nov), Ci(2 Nov), and Ci(25 Oct) distributions in Fu and Liou (1993), respectively.

The cloud extinction coefficient (β_{ext}), single-scattering albedo (ω), and asymmetry factor (g) from the parameterizations of Hu and Stamnes (1993) for water clouds, and Fu and Liou (1993) for ice clouds are averaged over each wavelength interval.

$$\begin{aligned} \bar{x}_i &= \frac{1}{(\lambda_i - \lambda_{i-1})} \int_{\lambda_{i-1}}^{\lambda_i} x(\lambda') d\lambda' \\ x &= \beta_{ext}, \omega, g \end{aligned} \quad (7)$$

The water cloud values are shown in Figures 1a, b, and c. The ice cloud values are shown in Figures 2a and b.

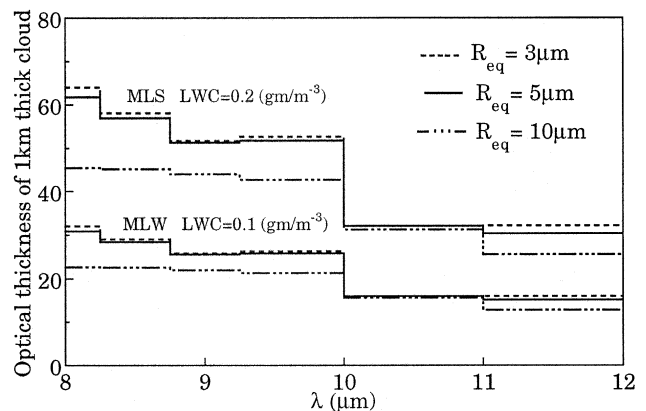


Figure 1a. Optical thickness of 1-km-thick water clouds, for MLS and MLW conditions.

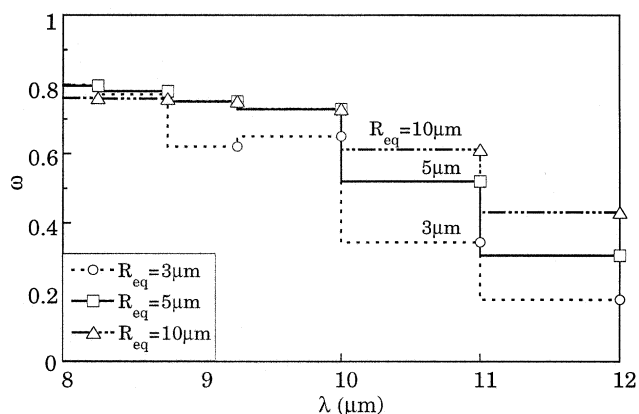


Figure 1b. ω for water clouds, various R_{eq} .

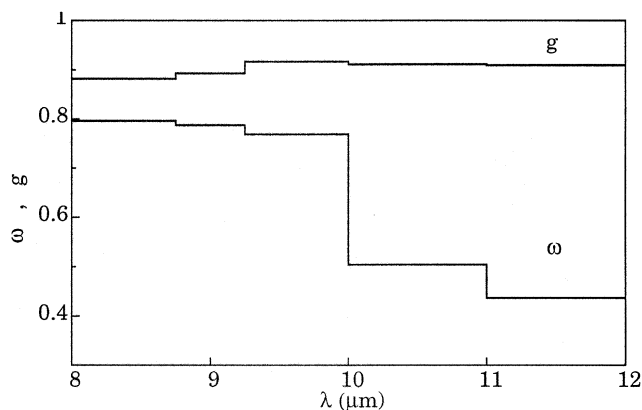


Figure 2b. ω and g for ice clouds.

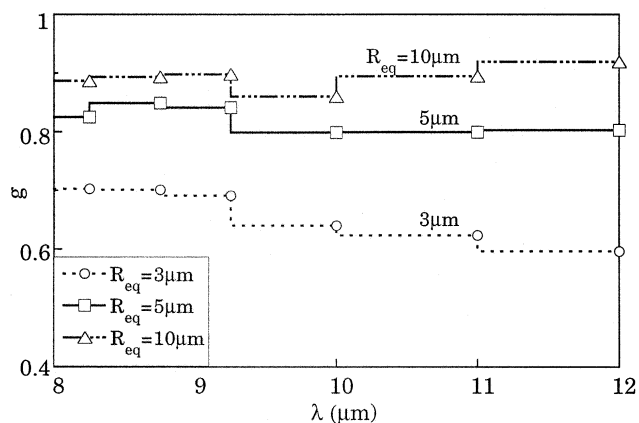


Figure 1c. g for water clouds, various R_{eq} .

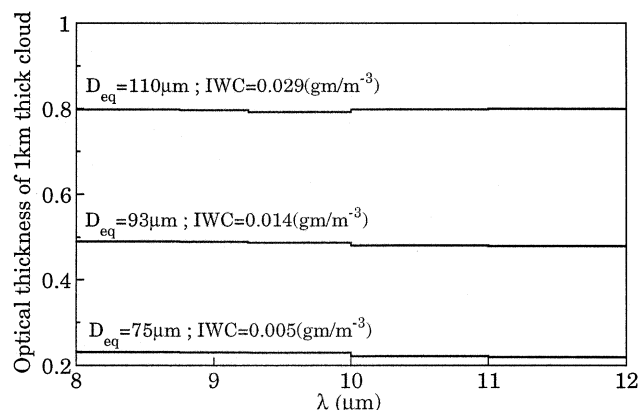


Figure 2a. Optical thickness of 1-km-thick ice clouds.

Results

The downward flux at the surface as a function of base cloud fraction (N) for the MLS and MLW atmospheres is shown in Figures 3a and b. Solid lines are used for the large clouds ($\alpha = 1$ $D = 1$ km), dashed lines for the small clouds ($\alpha = 0.5$ $D = 0.25$ km). Solid symbols are used for the water clouds, base altitudes of 0.5 km, 2 km, and 4 km; the open symbols are for ice clouds, base altitudes of 8 km, 10 km, and 12 km. The symbols are centered on the fluxes for $R_{eq} = 5\mu\text{m}$; and $D_{eq} = 93\mu\text{m}$ $\text{IWC} = 0.014\text{ g}\cdot\text{m}^{-3}$. This line and symbol convention is used in all subsequent figures. Limit bars show results for the other R_{eq} and D_{eq} - IWC pairs.

In Figure 3a (MLS) the fluxes range from a clear-sky ($N = 0$) value of $45\text{ W}\cdot\text{m}^{-2}$ to a high of $103\text{ W}\cdot\text{m}^{-2}$ for completely overcast 1-km-thick water clouds at base altitude 0.5 km. The water cloud fluxes decrease as cloud altitude increases. The limit bars are noticeable for the small water clouds but not for the large water clouds. The small water cloud flux decreases as R_{eq} increases. The variation in optical properties with R_{eq} is important for the small clouds but not the large clouds. This indicates that the large water clouds are opaque but the small water clouds are not. For completely overcast skies ($N = 1$), the fluxes for large and small water clouds with the same base altitude come close but do not match. The ice cloud fluxes vary slightly from the clear sky flux. There is a small increase in flux as the clouds get bigger. Flux variations with D_{eq} and IWC are less than $3\text{ W}\cdot\text{m}^{-2}$. Figure 3b (MLW) has a similar shape. The fluxes range from $8\text{ W}\cdot\text{m}^{-2}$ for clear skies to $69\text{ W}\cdot\text{m}^{-2}$. The water clouds behave as in Figure 4a, except that the fluxes at $N = 1$ are not close to matching. Again, the large water clouds are opaque and the ice cloud fluxes are nearly the same as the clear-sky flux.

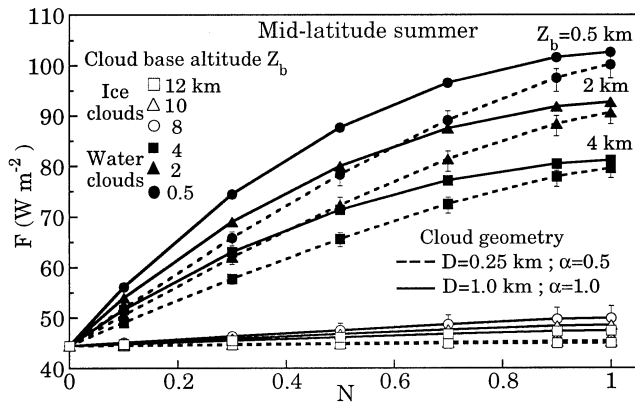


Figure 3a. MLS downward flux at surface for small and large clouds, various base altitudes (Z_b).

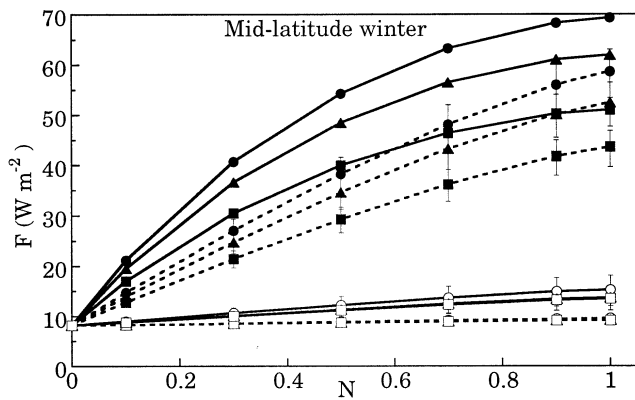


Figure 3b. MLW downward flux at surface.

The upward fluxes at 15 km for MLS and MLW are shown in Figures 4a and b. In Figure 4a, the fluxes range from $102 \text{ W}^*\text{m}^{-2}$, for clear skies, to $67 \text{ W}^*\text{m}^{-2}$ for large water clouds at 4 km. The water cloud fluxes decrease as cloud height increases. Small clouds have higher fluxes because their tops are lower at higher temperatures. As in Figure 3a, the small cloud fluxes vary with R_{eq} but the large cloud fluxes do not. The ice cloud fluxes group together according to cloud size. The small cloud fluxes are closely bunched, close to the clear sky flux, decreasing as cloud altitude and N increase. They do not show much dependence on D_{eq} and IWC because their optical thickness is quite small (<0.1 for the small clouds). The large ice cloud fluxes are loosely bunched, also decreasing as cloud altitude and N increase. Their fluxes vary considerably with D_{eq} and IWC. For $N = 1$, the flux for the 1 km thick ice cloud (open square solid line) is $78 \text{ W}^*\text{m}^{-2}$ ($D_{eq} = 93 \mu\text{m}$ IWC = $0.014 \text{ g}^*\text{m}^{-3}$) with an upper limit of $89 \text{ W}^*\text{m}^{-2}$ ($D_{eq} = 75 \mu\text{m}$ IWC = $0.005 \text{ g}^*\text{m}^{-3}$) and a lower

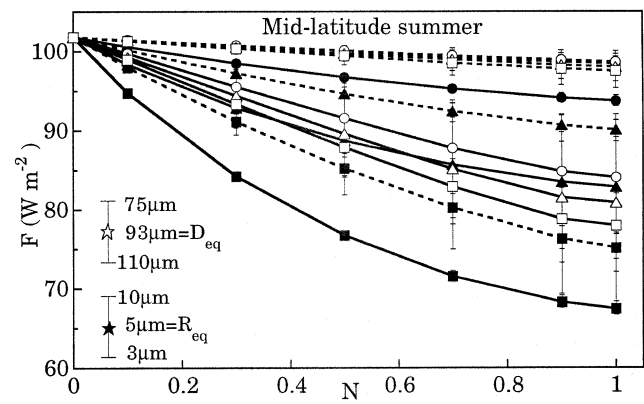


Figure 4a. MLS upward flux at 15 km.

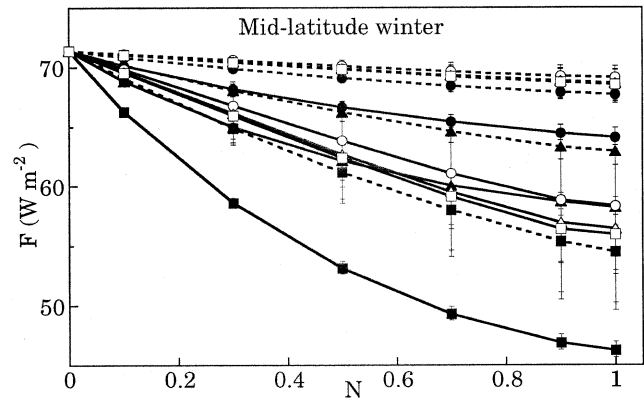


Figure 4b. MLW upward flux at 15 km.

limit of $68 \text{ W}^*\text{m}^{-2}$ ($D_{eq} = 110 \mu\text{m}$ IWC = $0.029 \text{ g}^*\text{m}^{-3}$). In Figure 4b, the fluxes show similar behavior, ranging from $71 \text{ W}^*\text{m}^{-2}$ to $46 \text{ W}^*\text{m}^{-2}$.

The errors for the flat plate and black cloud approximations are defined as

$$\delta F^{\uparrow\downarrow} = F^{\uparrow\downarrow}(\text{approximation}) - F^{\uparrow\downarrow} \quad (8)$$

The black cloud approximation was used for water clouds. The flat plate approximation was used for ice clouds. The error in the approximations for downward flux at the surface is shown in Figures 5a and b. There is no error for the clear sky case; the lines were not extended to zero at $N = 0$ in order to increase clarity.

In Figures 5a and b, the largest errors are due to using the black cloud approximation for small water clouds. The maximum error is $7.5 \text{ W}^*\text{m}^{-2}$ in Figure 5a (MLS) and

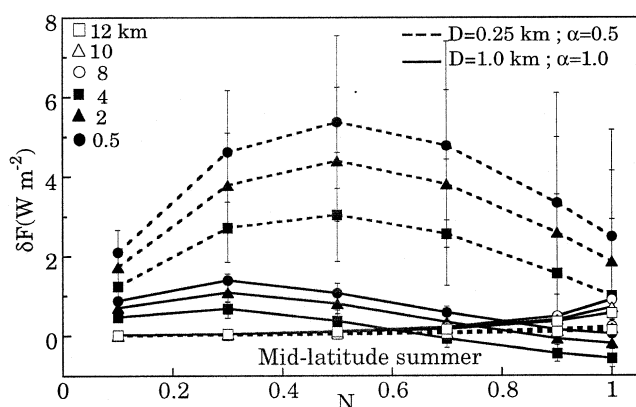


Figure 5a. MLS downward flux error at surface.

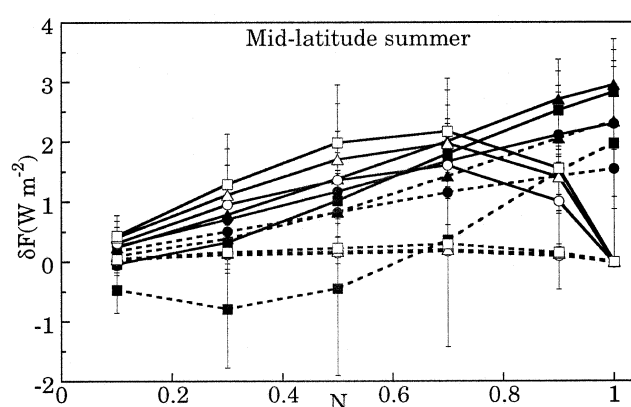


Figure 6a. MLS upward flux error at 15 km.

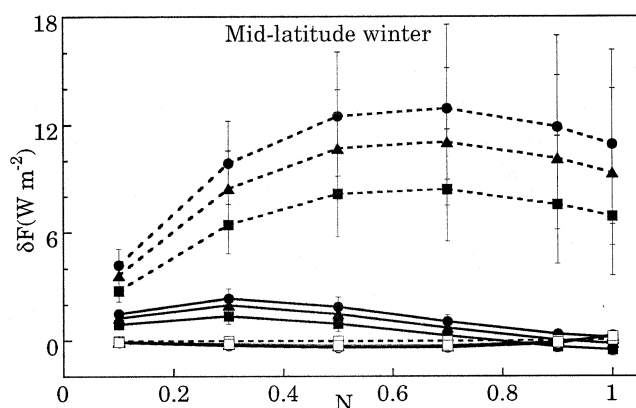


Figure 5b. MLW downward flux error at surface.

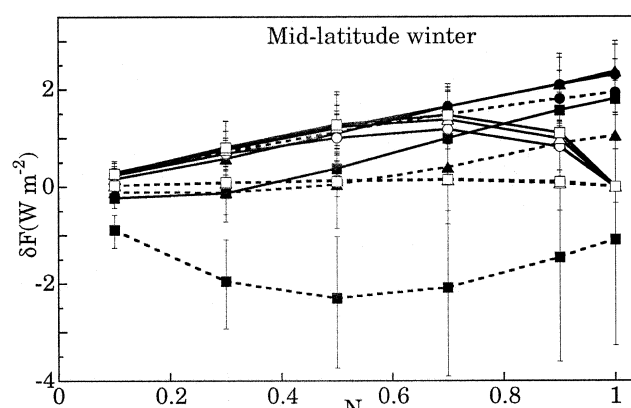


Figure 6b. MLW upward flux error at 15 km.

17.5 $\text{W}\cdot\text{m}^{-2}$ in Figure 5b (MLW). The error is due to transmission through the clouds. Because the small water clouds are not opaque, the surface “sees” the colder atmosphere above the clouds, resulting in lower fluxes at the surface. The errors for large water clouds are less than 3 $\text{W}\cdot\text{m}^{-2}$ in Figures 5a and b. Because the large water clouds are opaque, the transmission component of surface flux is negligible. The downward emission by the water clouds is augmented by the downward reflection from the cloud base, increasing the flux at the surface. This can be seen by noting that the error is slightly negative at $N = 1$. The augmentation by scattering increases the accuracy of the black cloud approximation. This agrees with the results of Han and Ellingson (1996), which showed that the black cloud assumption worked well for observed cumulus cloud fields. The maximum error for ice clouds is 1 $\text{W}\cdot\text{m}^{-2}$ in Figure 5a and 0.5 $\text{W}\cdot\text{m}^{-2}$ in Figure 5b. This is expected because ice clouds have little effect on the surface flux.

The errors for the upward flux at 15 km are shown in Figures 6a and b. The absolute value of the errors is less

than 4 $\text{W}\cdot\text{m}^{-2}$. There is very little error in the flat plate approximation for the small ice clouds; the maximum error is 0.5 $\text{W}\cdot\text{m}^{-2}$. This is expected because the clouds are relatively flat, $\alpha = 0.5$, and small. For the large ice clouds, maximum error is 3 $\text{W}\cdot\text{m}^{-2}$ at $N = 0.7$ in Figure 6a and 2 $\text{W}\cdot\text{m}^{-2}$ at $N = 0.7$ in Figure 6b. The largest water cloud errors are for the small water clouds at 4 km. The errors for those clouds are negative for $N < 0.9$ in Figure 6a and for all values of N in Figure 6b. In Figure 6b the error is -4 $\text{W}\cdot\text{m}^{-2}$ at $N = 0.7$. Because the error is negative, the actual flux is larger than that of a black cloud. This is a result of cloud transmission. Because the cloud top at 4.125 km is relatively cold, the upward transmission from the surface through the cloud is significant. For all other water clouds the error is positive. The large water clouds are opaque, so transmission is negligible. The other small water clouds are lower, so their emission is higher, making transmission less important.

Flux error profiles are shown in Figures 7a and b (MLS) for $N = 0.5$. Below the cloud layer, the downward flux error is

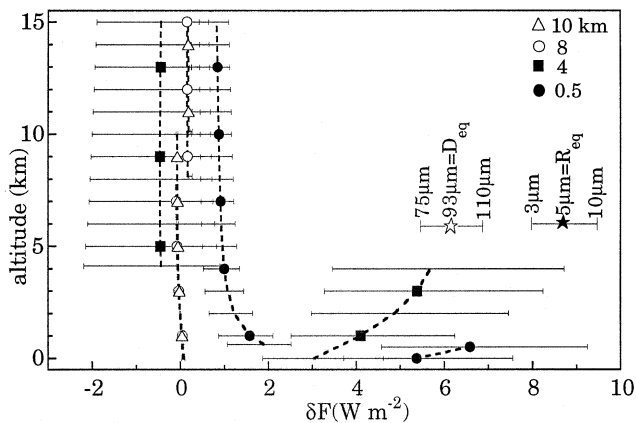


Figure 7a. MLS flux error profiles for small clouds, $D = 0.25$ km; $\alpha = 0.5$; $N = 0.5$.

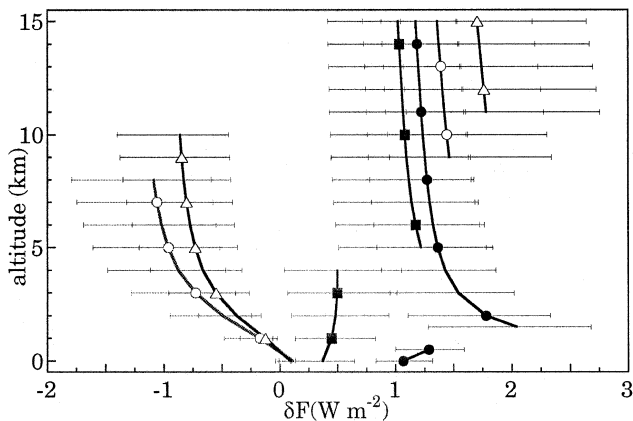


Figure 7b. MLS flux error profiles for large clouds, $D = 1$ km; $\alpha = 1$; $N = 0.5$.

plotted; above the cloud layer the upward flux error is plotted. There is no error in the upward flux below the clouds and the downward flux above the clouds. The smaller and larger clouds are separated and the 2 km and 12 km clouds are eliminated to increase clarity. The symbols and curves are for $R_{eq} = 5 \mu\text{m}$ and $D_{eq} = 93 \mu\text{m}$ $\text{IWC} = 0.014 \text{ g}\cdot\text{m}^{-3}$.

In Figure 7a the flux error profiles for the smaller flatter clouds ($\alpha = 0.5$; $D = 0.25$ km) are shown. The ice cloud errors are quite small, less than $\pm 0.5 \text{ W}\cdot\text{m}^{-2}$. The water cloud error ranges from $-2 \text{ W}\cdot\text{m}^{-2}$ to $9 \text{ W}\cdot\text{m}^{-2}$. The error is largest immediately above and below the cloud layer. The largest errors are for downward fluxes below the clouds. This is due to the partial transparency of the small water clouds. Note that the downward flux error decreases rapidly as the distance from the cloud base increases. The water

vapor emission below the clouds masks the error. Figure 7b shows the flux error profiles for the larger clouds ($\alpha = 1$; $D = 1$ km). The water cloud error is much smaller because the clouds are opaque. The ice cloud error is larger because the clouds are larger and not as flat, making geometry more important.

Conclusions

The black cloud approximation worked well for opaque water clouds; it failed when the clouds became partially transparent. If a simple nonscattering absorptivity was used for the partially transparent water cloud, the error would have been reduced. This contradicts the earlier conclusions in Takara and Ellingson (1996), which neglected gaseous absorption and emission. The flat plate approximation works well for the ice clouds considered. As expected, the approximation worked best for the smaller ice clouds that were more transparent and more flat. The accuracy of the flat plate approximation will decrease as the clouds become thicker or more opaque.

Acknowledgments

This paper was sponsored in part by the U.S. Department of Energy's Atmospheric Radiation Measurement (ARM) Program under grant DEFG0294ER61746.

References

- Clough, S. A., M. J. Iacono, and J. L. Moncet, 1992: Line-by-line calculations of atmospheric fluxes and cooling rates: Application to water vapor. *J. Geophys. Res.*, **97**, 15,761-15,785.
- Ebert, E. E., and J. A. Curry, 1992: A parameterization of ice cloud optical properties for climate models. *J. of Geophys. Res.*, **97**, 3831-3836.
- Ellingson, R. G., 1982: On the effects of cumulus dimensions on longwave irradiance and heating rates. *J. of Atmos. Sci.*, **39**, 886-896.
- Fu, Q., and K. N. Liou, 1993: Parameterization of the radiative properties of cirrus clouds. *J. of Atmos. Sci.*, **50**, 2008-2025.
- Han, D., and R. G. Ellingson, 1996: Validation of cumulus cloud parameterizations for longwave radiation calculations. In *IRS '96: Current Problems in Atmospheric Radiation.*, W. L. Smith and K. Stamnes, eds., 230-233.

Harshvardhan, and J. A. Weinman, 1982: Infrared radiative transfer through a regular array of cuboidal clouds. *J. of Atmos. Sci.*, **39**, 431-439.

Howell, J. R., and M. Perlmutter, 1964: Monte Carlo solution of thermal transfer through radiant media between gray walls. *J. Heat Transfer*, **86**, 116-122.

Hu, Y. X., and K. Stamnes, 1993: An accurate parameterization of the radiative properties of water clouds suitable for use in climate models. *J. of Climate*, **6**, 728-742.

Kiehl, J. T., 1992: Atmospheric circulation models. *Climate System Modeling*, K. E. Trenbreth ed., Cambridge University Press, 344.

McClatchey, R. A., R. W. Fenn, J. E. A. Selby, F. E. Volz, and J. S. Garing, 1971: Optical properties of the atmosphere (rev.). *Rep. AFCRL-71-0279*, 85 pp., Air Force Cambridge Research Laboratory, Bedford, Massachusetts.

Takara, E. E., and R. G. Ellingson, 1996: Scattering effects on longwave fluxes in broken cloud fields. *J. of Atmos. Sci.*, **53**, 1464-1476.